

Article

Synthesis of an Aryl-Semicarbazone-Based Cu(II) Complex for DNA and BSA Interaction and Anti-Cancer Activity against Human Cervix Uteri Carcinoma

Ribhu Maity¹, Biplab Manna¹, Swapan Maity², Kalyanmoy Jana¹, Tithi Maity³, Mohd Afzal^{4,*}, Nayim Sepay⁵ and Bidhan Chandra Samanta^{1,*}

¹ Department of Chemistry, Mugberia Gangadhar Mahavidyalaya, Bhupatinagar, Purba Medinipur 721425, West Bengal, India; maityribhuj@gmail.com (R.M.); biplabmanna2245@gmail.com (B.M.); kalyanmoyjana@gmail.com (K.J.)

² School of Materials Science and Technology (SMST), Indian Institute of Technology (IIT), Banaras Hindu University, Varanasi 221005, Uttar Pradesh, India; swapanmaity.rs.mst19@itbhu.ac.in

³ Department of Chemistry, Prabhat Kumar College, Contai 721401, West Bengal, India; tithi_maity@yahoo.co.in

⁴ Department of Chemistry, College of Science, King Saud University, Riyadh 11451, Saudi Arabia

⁵ Department of Chemistry, Lady Brabourne College, Kolkata 700017, West Bengal, India; nayimsepay@yahoo.com

* Correspondence: maslam1@ksu.edu.sa (M.A.); bidhansamanta@yahoo.in (B.C.S.)

Abstract: The current study provides an in-depth analysis of the biological properties of a Cu(II) complex ($C_{22}H_{24}Cu_2N_6O_{10}$) obtained from an aryl-semicarbazone ligand derived (L) from the condensation of 2,4-dihydroxy acetophenone and semicarbazide. The binding behavior of this complex with calf thymus DNA (CT-DNA) and bovine serum albumin (BSA) protein was explored using a combination of experimental and theoretical approaches. The results suggest that the complex binds with CT-DNA via a partial intercalation, and hydrophobic interaction. However, the complex binds to BSA protein predominantly through hydrogen bonding or van der Waals interactions rather than hydrophobic interactions. The molecular docking methodology was carried out to substantiate the experimental finding. Furthermore, the in vitro cytotoxicity study was conducted on human cervix uteri carcinoma (SiHa cancerous cell) lines upon exposure to the complex, and the findings reveal a considerable decrease in cell viability, when compared to the control. Overall, this study provides a comprehensive understanding of the biological potential of the Cu(II) complex and its potential as an anti-cancer agent.

Keywords: Cu(II) complex; aryl-semicarbazone ligand; DNA/BSA interaction; cytotoxicity; SiHa cancer cell



Citation: Maity, R.; Manna, B.; Maity, S.; Jana, K.; Maity, T.; Afzal, M.; Sepay, N.; Samanta, B.C. Synthesis of an Aryl-Semicarbazone-Based Cu(II) Complex for DNA and BSA Interaction and Anti-Cancer Activity against Human Cervix Uteri Carcinoma. *Inorganics* **2024**, *12*, 19. <https://doi.org/10.3390/inorganics12010019>

Academic Editors: Luciano Saso and Irena Kostova

Received: 11 November 2023

Revised: 23 December 2023

Accepted: 29 December 2023

Published: 1 January 2024



Copyright: © 2024 by the authors. Licensee MDPI, Basel, Switzerland. This article is an open access article distributed under the terms and conditions of the Creative Commons Attribution (CC BY) license (<https://creativecommons.org/licenses/by/4.0/>).

1. Introduction

The research trends for developing chemotherapy metal-based agents are now shifted from platinum-based complexes [1–3] to non-platinum-based complexes involving titanium, gallium, germanium, palladium, gold, cobalt, ruthenium, tin, etc., to reduce the side effects of platinum-based drugs, which had been serving predominantly as anti-cancer drugs for a long period [4–6]. A considerable number of research articles proved that copper(II)-based complexes are also eligible to act as promising anti-cancer agents with comparatively low toxicity and side effects [7,8]. It is essential to choose suitable ligands because the biological activity of these ligands contributes significantly to the overall properties of biologically active complexes [9,10].

For instance, semicarbazone is an important pharmacophore in the search for new drugs [9,11]. The transition metal complexes with semicarbazone exhibit significant biological activity as the ligand, semicarbazone, itself has huge potential to act as a biologically

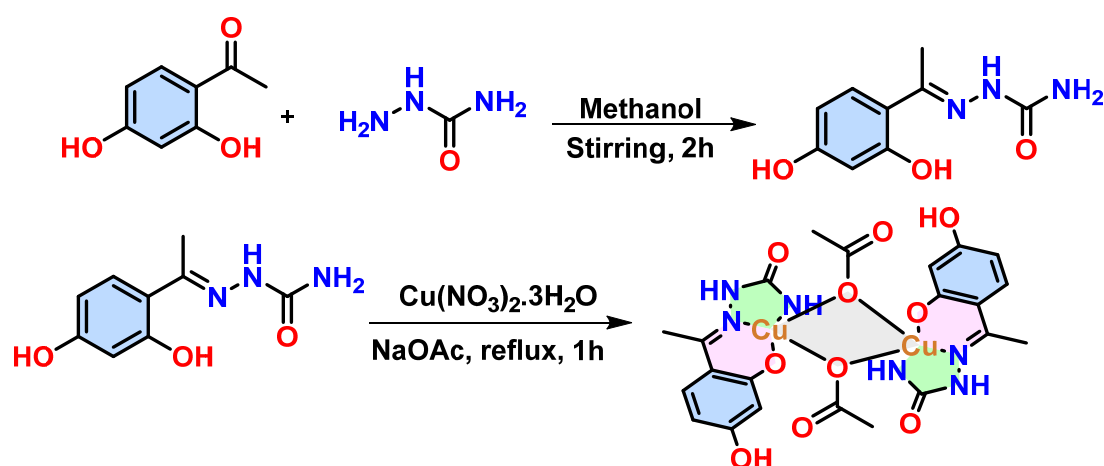
active reagent [12]. In particular, in terms of biological importance, Cu(II) complexes containing semicarbazone are found to exhibit potential anti-cancer properties by prompting apoptosis and intercalation into the DNA helix [13]. The ability of metal complexes to bind DNA is tuned by several parameters, including ligand planarity, donor atom, and coordination geometry [14]. Interaction between metal complexes and bovine serum albumin (BSA) has also gained significant momentum to explore their cytotoxic properties as BSA is highly similar to human serum albumin (HSA) and is stable, low cost, and possesses inherent fluorescence emission capability [15]. Thus, to develop a potential metal-based anti-cancer entity, it is very crucial to unveil the binding interaction of metal complexes with DNA and BSA.

The present investigation aimed to synthesize a Cu(II) complex using aryl-semicarbazone derivatives to evaluate its cytotoxicity activity against SiHa cancer cell lines and prospective binding interaction efficacy with CT-DNA and BSA protein.

2. Results and Discussions

2.1. Synthesis

The synthesis route for the ligand and the copper complex is shown in Scheme 1.



Scheme 1. Scheme for the synthesis of ligand and its copper(II) complex.

The complex formed by refluxing a Schiff-base ligand and copper nitrate [$\text{Cu}(\text{NO}_3)_2 \cdot 3\text{H}_2\text{O}$] in dimethyl formamide (DMF) solution in a 2:1 molar ratio. Although it started from nitrate, sodium acetate was used as base in the synthesis; and as a result, the isolated species contains acetate as a ligand. The deep green solid precipitate formed was filtered off and dried in vacuo. The complex showed good solubility in dimethyl sulfoxide (DMSO) and MeOH. The ligand to metal ratio and purity of the complex and free ligand were confirmed by the elemental analysis (given in experimental section).

2.2. Spectroscopic Studies

2.2.1. UV–Vis Spectroscopy

Due to the lack of crystals suitable for single-crystal X-ray crystallography, the structural establishment of the complex was performed by spectroscopic and semiempirical methods. The complex showed two characteristic absorption peaks between 274 and 319 nm and the ligand showed only one peak at 343 nm (Supplementary Information, Figures S1 and S2). The high-energy band at 274 nm is due to the $\pi \rightarrow \pi^*$ intra-ligand charge transfer (ILCT) transition, while the band at 319 nm was assigned to the ligand-to-metal charge transfer (LMCT) transition. Therefore, the results indicate the attachment of the metal ion with the ligand.

2.2.2. FTIR Spectroscopy

In the FTIR spectrum (Figure S3a) of the complex, the four major indicative bands appeared which include $\nu(\text{C}=\text{N})$, $\nu(\text{C}-\text{O})$, $\nu(\text{Cu}-\text{O})$, and $\nu(\text{Cu}-\text{N})$. The stretching band appeared at 1656, and 1220–1227 cm^{-1} , signifying the involvement of azomethine nitrogen and phenolic oxygen with the copper(II) center, respectively. The N-H stretching appeared at 3250 cm^{-1} . The peaks at 3144 cm^{-1} , and 2810 cm^{-1} were for aromatic C-H and aliphatic C-H stretching of the complex, respectively. The stretching bands at 477 and 444 cm^{-1} in the spectrum assigned to $\nu(\text{Cu}-\text{O})$ and $\nu(\text{Cu}-\text{N})$, respectively, indicate the phenoxide (O^-) and imine ($\text{C}=\text{N}$) groups of ligand coordinated to Cu(II) ion in the complex formation.

The ligand's IR spectral data (Figure S3c) reveal a distinctive absorption peak at 1611 cm^{-1} corresponding to the azomethine moiety ($\text{C}=\text{N}$), indicative of Schiff base formation. In the complex, this azomethine peak undergoes a shift to 1656 cm^{-1} , attributed to the coordination between the azomethine nitrogen and the metal center. Additionally, the free ligand exhibits a prominent band at 1026 cm^{-1} associated with the phenolic Ar-O group. In the complex spectrum, this band shifts to a lower frequency (1015 cm^{-1}), highlighting the coordination of the metal ion through the deprotonated phenolic oxygen atoms. The strong bands at 1630 and 1440 cm^{-1} may be assigned for acetate ($-\text{COO}^-$) symmetric and asymmetric stretching [16], respectively. Further, the absorption spectrum bands of semicarbazone ligand in infrared radiation (IR) include three characteristic bands at 1600–1650 cm^{-1} , 1470–1570 cm^{-1} and 1250–1350 cm^{-1} . All these bands strongly support the formation of the complex.

2.2.3. Mass Spectroscopy

The ESI-MS spectrum has provided more evidence for the complex's formation (Figure S4). A clear peak at 681.0118 matches well with the m/z values of the proposed formula with Na^+ ion ($m/z = 681.0038$), consistent with the schematic structure of the complex. Further, the intense peak at 701.49 seems to have isotopic Cu structure and as result could be the molecular one. Also, the most intense peak at m/z 274.27 is a stable fragment in mass spectra containing a monomeric structure of the complex without acetate bridging but with some adducts like methanol, ammonium ion, H^+ or methyl cyanide generally occurring during the mass experiment.

2.3. Theoretical Analysis

The density functional theory (DFT) has been employed to determine the complex's structure. The DFT is used to optimize the predicted structure and it was validated through matching of DFT-simulated and experimental IR spectra. This study reveals a binuclear copper complex of (E)-2-(1-(2,4-dihydroxyphenyl)ethylidene)hydrazine-1-carboxamide. The metal atoms are joined by two acetate bridging and the predicted structure is presented in Figure 1a. It is found that all the Cu-O and Cu-N bond lengths are in the range of experimental values (Table S1). The predicted structure of the complex was validated by matching the experimental and DFT-simulated IR spectroscopy (Figure S3b). Most of the peaks of the complex have been fitted well with the experimental data (Table S2) indicating the perfection of the structure.

Further, using the DFT method, the reactivity of the complex can also be understood. The molecular orbital having the highest energy (i.e., HOMO) is most important if the complex interacts with the molecule in its vicinity through electron donation. In this case, the HOMO is concentrated mainly on both the metal centers of the complex. Again, the complex can also interact with other molecules through electron acceptance. Here, the lowest unoccupied molecular orbital (LUMO) is the key orbital. In this complex, the LUMO is distributed over the entire molecule (both the metal ion as well as aromatic moieties). The low HOMO-LUMO gap (2.26 eV, Figure 1b) indicates that the molecule has a high capability to interact with other molecules.

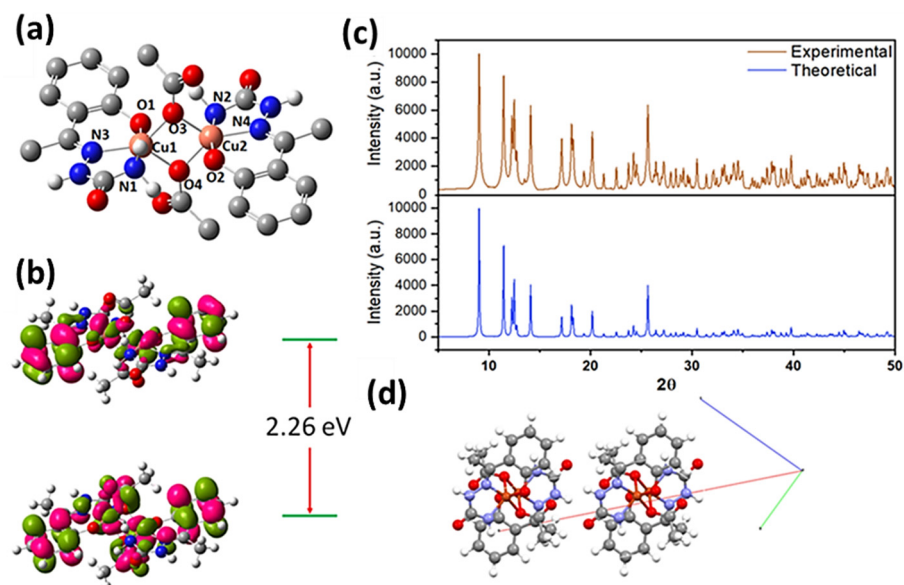


Figure 1. (a) Predicted structure of the complex, (b) HOMO-LUMO gap in the DFT study, (c) experimental and simulated powder X-ray pattern, and (d) the crystal packing of the complex.

The crystal of the complex is not the quality required for single-crystal X-ray crystallography. A powder X-ray crystallographic study was performed to get a structural insight into the compound. Now, in the solid state, the complex will take one of the possible space groups. Using the DFT energy minimized structure, all the possible unit cells were calculated and powder X-ray patterns were simulated for each calculated unit cell. Now the matching of the simulated powder X-ray pattern and experimental pattern will provide the most probable crystal packing and the structure of the complex. The results show that the experimental powder X-ray pattern fits very well with the powder X-ray pattern of the complex packed in a triclinic crystal system with a P-1 space group (Figure 1c). The unit cell parameters were found to be $a = 23.2555$, $b = 8.0258$, and $c = 13.8639$ for lengths and $\alpha = 52.3294$, $\beta = 46.4030$, and $\gamma = 44.1513$ for angles. The crystal packing of the complex is shown in Figure 1d.

2.4. Solution Stability and Lipophilicity

We used UV-vis spectroscopy to confirm the stability of the metal complex before examining the DNA/BSA binding and cytotoxicity studies in solution state. The result confirms the complex's long-term stability in a buffer solution (Figure S1).

Lipophilicity is an essential characteristic of molecules to acquire evidence about cytotoxicity, diffusion, and accumulation of the considered molecule in the cell membranes. It can be quantitatively evaluated through $\log P_{o/w}$ values [17]. The literature review suggests that for most of the cytotoxic molecules, the lipophilicity value ranges between -0.4 to 5.6 (on average 2.52) [18]. Herein, the $\log P_{o/w}$ value for the complex is obtained as 0.06 , which is greater than the $\log P_{o/w}$ value of cisplatin (-2.28 ± 0.07), indicating that the studied complex is significantly lipophilic. These observations are reflected in the experimental results of cytotoxicity studies performed for the complex (discussed later on).

2.5. DNA Binding

2.5.1. Electronic Absorption

The changes in the spectra of Cu(II) complex for a particular amount were noted in the presence of successive addition of CT-DNA (0 – $11.66 \mu\text{M}$) (Figure 2a). Figure 2a demonstrates hyperchromism at 319 nm , which might be due to electrostatic binding [19] or partial straightening out of the DNA helix [20]. On the other hand, there was a gradual decrease in the maxima at 274 nm with the increase in the concentration of CT-DNA. Further, the intrinsic binding constant (K_{ib}) value ($4.70 \times 10^5 \text{ M}^{-1}$) has been determined from the

plot of $[DNA]/(\epsilon_a - \epsilon_f)$ vs. $[DNA]$ (Figure 2b). The obtained K_{ib} value is close to the power of ethidium bromide (a classical intercalator; $4.94 \times 10^5 \text{ M}^{-1}$). These observations suggest that the complex avidly binds to DNA [21].

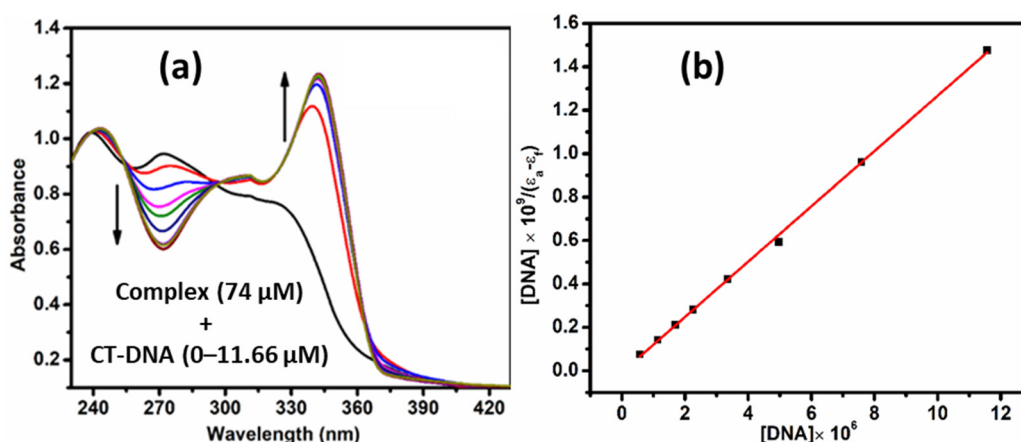


Figure 2. (a) Absorption spectrum of the complex (74 μM) in the presence of CT-DNA (0–11.66 μM). (b) Plot of $[DNA]/(\epsilon_a - \epsilon_f)$ vs. $[DNA]$ for determining K_{ib} .

2.5.2. Emission Studies

The emission studies have been monitored at 514 nm, at which the present complex shows emission in the absence of DNA. However, in the presence of CT-DNA, a significant enhancement in emission profile has been observed at different temperatures, indicating probable interaction of the complex with DNA (Figure 3). The enhancement constant could be measured using Equation (1) [22]:

$$F_0/F = 1 - K_E[E] \quad (1)$$

where F_0 and F denote the fluorescence intensity in the absence and presence of the complex, respectively. K_E is the enhancement constant, and $[E]$ is the concentration of the complex. From the slope of plotting F_0/F vs. $[E]$, the K_E value is determined and the enhancement constants at 298, 303, and 308 K are given in Table S3. From double-log plot Equation (2), the binding constants (K_b) at 298, 303, and 308 K were also determined (Table 1). The binding constant values obtained from the current experiments are very much comparable with the reported other Cu(II) complexes [23–26].

$$\log [(F_0 - F)/F] = \log K_b + n \log [\text{complex}] \quad (2)$$

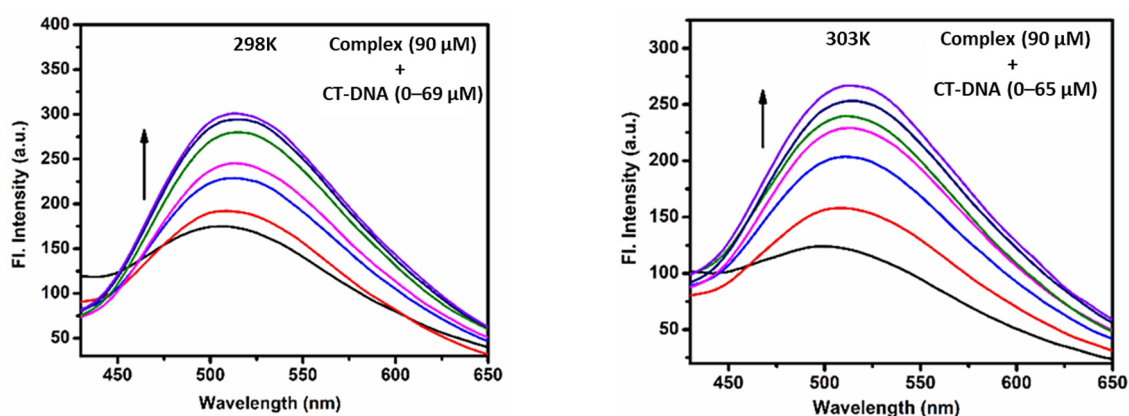


Figure 3. Cont.

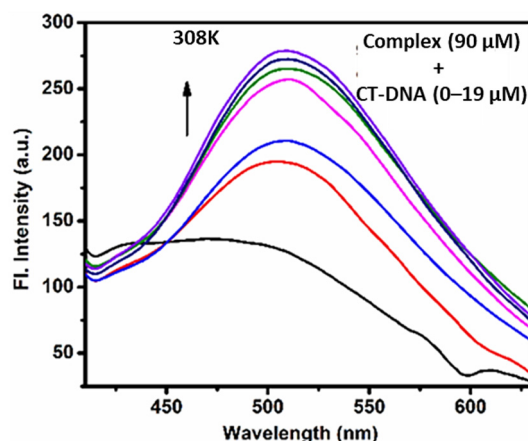


Figure 3. Emission profile of complex alone, and in the presence of CT-DNA at 298, 303, and 308 K.

Table 1. Binding parameters of complex–DNA interaction.

Temperature (K)	K_b	ΔG (kJ mol ^{−1})
298	7.128×10^4	−27.68
303	2.44×10^5	−31.24
308	4.72×10^5	−33.41

2.5.3. Determination of Enthalpy and Entropy Changes (ΔH and ΔS)

The thermodynamic parameters (ΔH and ΔS) have been calculated employing van't Hoff's Equation at studied temperatures (Figure 4). The plot of $\ln K_b$ vs. $1/T$ gives the value of ΔH and ΔS for complex–DNA interaction as 143.91 kJ/mol and 358.76 J/mol K, respectively. These values suggest that the studied complex interacts with DNA in a hydrophobic manner [27] rather than through hydrogen bonding or Van der Waals interactions, and the complex's spontaneous interaction with DNA is supported by the negative ΔG value (Table 1).

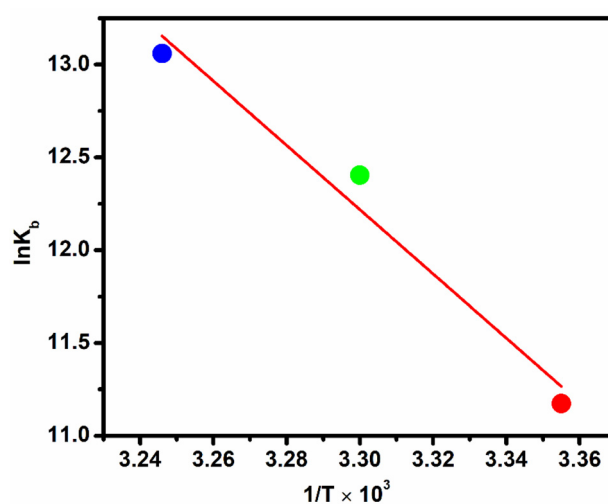


Figure 4. Plot of $\ln K_b$ vs. $1/T$ for the complex.

2.5.4. Binding Mode

To conclude the binding mode between the complex and DNA, comparative binding analysis, fluorescence spectroscopy, helix melting viscosity measurement, and influence of salt concentration were undertaken.

We performed a comparative binding analysis with ethidium bromide (EB) (intercalating agent), and with Hoechst (groove binder) to analyze the binding mode of the complex

with DNA. For this purpose, the DNA (18 μM) was mixed with the complex (119 μM) and titrated with EB to execute the fluorescence displacement assay of the complex by EB (Figure S5). Before the experiment, the samples were incubated with EB for 5 min. A similar assay of the complex by Hoechst was also monitored using DNA pre-bound with the complex (Figure S6). In this case, also DNA (18 μM) was complexed with the maximum concentration of the complex (119 μM) and titrated with Hoechst (0–28 μM).

From these comparative displacements, the DC_{50} values (concentration required to dislodge 50% from the complex–DNA system by the respective EB and Hoechst) were determined to assess the comparative involvement of intercalation or groove binding. It is observed that for EB, the DC_{50} value is near 31 μM , whereas no such significant replacement of the complex by Hoechst from DNA complex adduct is observed. This demonstrates that complex binds with DNA via a partial intercalation.

Usually, the intercalation mode of binding causes an increase in the helix melting temperature (T_m) (>5 $^{\circ}\text{C}$) for the DNA, because it provides more stability to the DNA than the rest of the binding mode [28]. On the contrary, a subtle change in the T_m value was observed in the case of groove and electrostatic binding mode [29]. The experiment showed that upon binding with the complex, the T_m of DNA is increased by ~ 5.25 $^{\circ}\text{C}$ (not so high increase), which established the partial intercalation binding mode (Figure S7).

Viscosity measurement is also a reliable method to ensure the binding mode of the complex with DNA [30]. The viscosities of the DNA (0.029 μM) were determined in the absence and presence of increasing concentrations of EB (0.01–0.05 μM), complex (0.01–0.05 μM), and Hoechst (0.01–0.05 μM). The relationship between the relative solution viscosity (η/η_0) and DNA length (L/L_0) is shown by Equation 3;

$$L/L_0 = (\eta/\eta_0)^{1/3} \quad (3)$$

where L and L_0 are the apparent molecular lengths in the presence and absence of the compound, respectively. The obtained data are presented as $(\eta/\eta_0)^{1/3}$ vs. r , where η is the viscosity of the DNA in the presence of EB or the complex or Hoechst, η_0 signifies the viscosity of the DNA alone in the buffer solution, and r is the $[\text{EB}]$ or $[\text{complex}]$ or $[\text{Hoechst}]/[\text{DNA}]$ ratio.

The plots of relative viscosities of the CT–DNA–EB, CT–DNA–Hoechst, and CT–DNA–complex systems with increasing concentrations of EB, Hoechst, or complex shows the increase in the relative viscosity of the CT–DNA complex adduct (Figure S8). However, the observed changes for the complex–DNA interaction were less than that for EB, indicating partial intercalation.

It has been noted that certain ligands may bind to DNA in a non-specific way through electrostatic interactions in addition to intercalative and groove binding [31]. We studied the effect of salt concentration on complex–DNA binding to Figure out the possible role of the electrostatic interaction between them. The association constants (K_b) of the complex (30 μM) with the gradual addition of DNA were obtained at different NaCl concentrations (25–100 μM).

The log of the binding constant K_b is represented by the Equation (4):

$$\log(K_b) = \log(K_{\text{nel}}) - Z\Psi \times \log[\text{NaCl}] \quad (4)$$

where Z = number of oxygen phosphate groups engaging with the ligand, $Z\Psi$ = total number of tightly bound cations released, and $\Psi = 0.88$, which is the number of Na^+ ions released upon ligand binding per phosphate group [32].

The value of $Z\Psi$ and Z was found to be 0.962 and 1.09, respectively, reflected from the plot of $\log K_b$ vs. $\log [\text{NaCl}]$ (Figure S9). The ΔG_{el} and ΔG_{nel} were observed as -6.73 and -22.99 kJ/mol resulting in a total ΔG of -29.72 kJ/mol, demonstrating the spontaneity of the process. It was discovered that there was significantly less electrostatic constituent of the Gibbs free energy when compared to the non-electrostatic component, suggesting a

hydrophobic rather than electrostatic character of interaction. This observation has also been obtained from thermodynamic parameter calculation.

2.6. Binding Affinity with BSA

The absorption studies were performed in the absence and presence of various concentrations of BSA (0–0.34 μM) to the fixed amount of complex (74 μM) as shown in Figure 5a. On incremental addition of BSA, the absorption intensity of the complex at 319 nm is continually increased but it decreased at 274 nm because of the interaction between the complex and BSA. Isosbestic points at 257 and 293 nm direct the occurrence of reversible binding phenomena. The apparent association constant (K_{app}) was achieved by implementing the following Equation (5):

$$1/(A_{\text{obs}} - A_0) = 1/(A_c - A_0) + 1/K_{\text{app}}(A_c - A_0)[\text{complex}] \quad (5)$$

where A_{obs} is the observed absorbance of the solution, A_0 is the absorbance of BSA alone, and A_c is the absorbance of BSA bound complex. The K_{app} value calculated from the plot (Figure 5b) is 4.37×10^4 , which is in consistent with the reported copper(II)-Schiff base complexes [33].

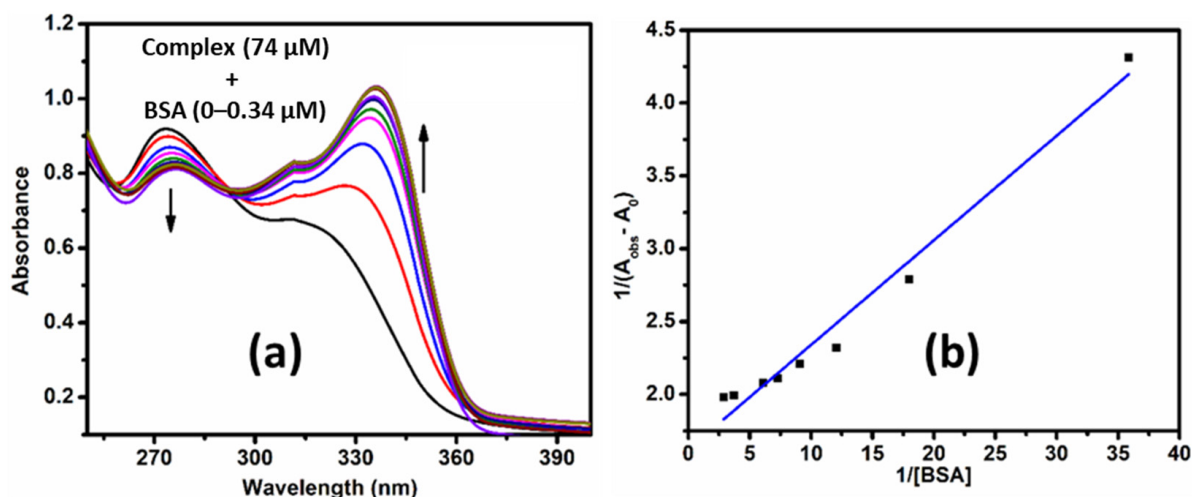


Figure 5. (a) Absorption spectrum of the complex (74 μM) in the presence of BSA (0–0.34 μM). (b) Plot of $1/[\text{BSA}]$ vs. $1/(A_{\text{obs}} - A_0)$ for the BSA to complex.

With the addition of the complex, the emission profile of BSA (at approximately 335 nm) exhibits fluorescence quenching at 298, 303, and 308 K (Figure S10). Involving Equations (6) and (7), the results were analyzed.

$$F_0/F = K_{\text{SV}}[Q] + 1 \quad (6)$$

$$K_{\text{SV}} = K_q \tau_0 \quad (7)$$

where τ_0 is the lifetime of the fluorophore in the absence of the quencher.

The observed Stern–Volmer constants (k_{sv}) at the three temperatures are presented in Table S4. Taking into account that the serum albumin τ_0 is close to 5×10^{-9} s, the quenching constant K_q value obtained is in the order of 10^{14} . A linear plot between F_0/F vs. $[Q]$ implies that the interaction between complex and BSA has been governed through a single quenching mechanism, which is the static mechanism (Figure S11). The binding constants (K_b) and the number of binding sites (n) per BSA calculated from Equation 4 are given in Table S4. A straight line is produced when the $\log((F_0 - F)/F)$ vs. $\log[\text{complex}]$ for all three temperatures is plotted (Figure S12).

Enthalpy (ΔH) and Entropy (ΔS) Determination

By virtue of van't Hoff's equation, these parameters were determined at different temperatures. Figure S13 depicts the plot of $\log K_b$ vs. $1/T$. The negative values for both ΔH and ΔS (-84.83 and -171.64 J/mol/K, respectively) of the complex–BSA interaction indicate hydrogen bonding or van der Waals interactions instead of hydrophobic interactions. Apart from this, negative free energy change (Table S4) shows the spontaneous nature of the interaction reaction between the complex and BSA.

2.7. Molecular Docking with DNA and BSA

Molecular docking is one of the most used computational skills to identify the binding region of a molecule in the macromolecule, the forces involved in their binding process, and the mechanism of their interaction [34]. For this reason, the method is applied to comprehend the behavior of the complex involving the DNA and BSA protein. The binding energy of the complex with the mentioned macromolecules is -6.16 and -7.35 kcal/mol, respectively. Therefore, the molecule has a higher binding affinity to the BSA concerning the DNA, which was also found in the experimental observations.

When it comes to DNA, the complex recognizes itself as the main groove (Figure 6a). Here, the molecule interacts with C3, G4, A5, A18, and T19 nucleotides (Figure 6b). It is interesting to note that the complex has hydrogen bonds with G4, A5, A18, and T19 nucleotides. However, the benzene ring and methyl group in the molecule interact with C3, G4, and A5 through $\pi \dots \pi$ (pink), N-H $\dots \pi$ (cyan), and C-H $\dots \pi$ (light pink) interactions (Figure 6b). The number of such interactions is higher than that of the H-bond. Therefore, the molecule prefers hydrophobic interactions over H-bonding in the DNA-binding process which is also found experimentally.

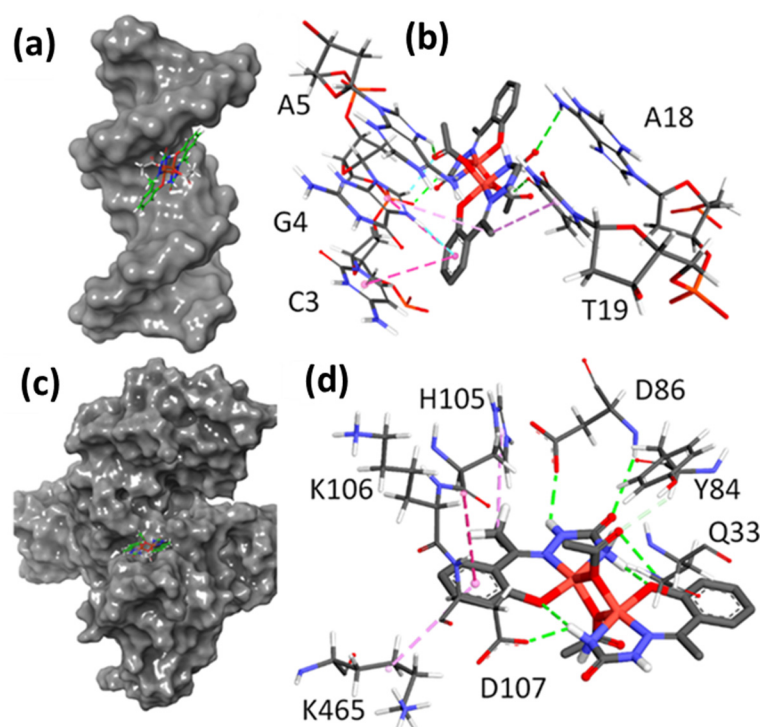


Figure 6. Docked pose of the complex with DNA (a,b) and BSA (c,d).

For BSA, the interaction process of the complex is more interesting as it was bound at the surface of the protein (Figure 6c). Here, the polar interactions are the key factor in the binding properties of the molecule. The complex has only two π -alkyl interactions with H105 and K465 (Figure 6d). One amide $\dots \pi$ interaction with K106 was observed here. Amino acid residues Q33, Y84, D86, and D107 (Figure 6d) interacted with the complex

through H-bond. Therefore, the hydrogen bonding interactions are found to be crucial for the protein binding process of the complex as found experimentally.

2.8. Cytotoxicity Studies with SiHa Cell Lines

Using an MTT assay, the cytotoxicity and inhibition of cell proliferation were studied in vitro through incubation of the cancer cells with a fixed complex concentration for 1, 2, and 3 days. Cultured cells in the absence of specimens are used as controls. To evaluate the efficiency of the complex, a concentration of approximately 50 $\mu\text{g}/\text{mL}$ was used (Figure S14). According to the cytotoxicity analysis, both ligand and complex showed moderate cytotoxicity against SiHa cells with IC_{50} $52.18 \pm 15.16 \mu\text{g}/\text{mL}$ and $41.75 \pm 11.40 \mu\text{g}/\text{mL}$, respectively. Here, the complex has better performance than that of the free ligand. Studies showed that a significant reduction in cell viability is observed on exposure of the complex in cancer cell lines than the control with cell apoptosis as evident from the fluorescent representation (Figure 7). The cell proliferation on the specimen using DNA binding dyes such as acridine orange (AO) and ethidium bromide (EB) dye reveals its cytotoxic nature. Both the dye can recognize normal cells from apoptotic cells based on the permeability of the cell membrane. Frequently, dead cells are permeable to both the dyes and fluoresce red while the living cells permeate only AO and fluoresce in green. Another interesting observation is that the cell's color gradually changes from green to yellow after treatment, indicating cell apoptosis from day 1 to 3 [35]. That is, the complex is highly cytotoxic and has the potential to act as a chemotherapeutic moiety.

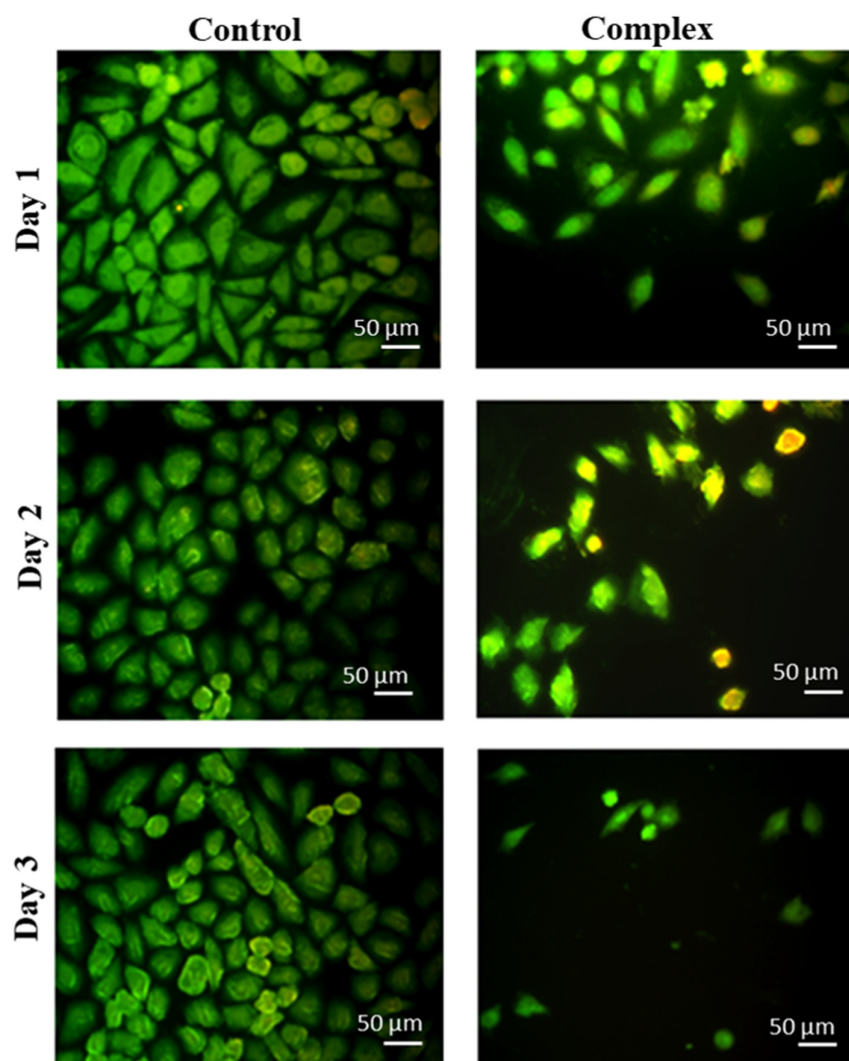


Figure 7. Fluorescent images of AO/EB staining of complex and control at days 1, 2, and 3.

3. Experimental Section

3.1. Materials

Methanol, DMF, 2, 4-dihydroxy acetophenone, semicarbazide, $\text{Cu}(\text{NO}_3)_2 \cdot 3\text{H}_2\text{O}$, and sodium acetate were purchased from Merck. BSA, CT-DNA, and ethidium bromide (EB) were procured from Sigma-Aldrich Chemicals Co. (Bengaluru, India) 4-(2-(419 hydroxyethyl)-1-piperazineethanesulfonic acid (HEPES) buffer of pH 7.14 was utilized to prepare the reagent solutions needed for biological investigations. It was routinely performed to dry analytical samples at room temperature in vacuo prior to analysis. There were two Perkin-Elmer 2400 Series II C, H, N analyzers used to record microanalytical data for the current study.

3.2. Ligand Preparation

The ligand and aryl-semicarbazone were prepared from the mixture of 2, 4-dihydroxy acetophenone (0.01 mol) and semicarbazide (0.01 mol) by stirring in 30 mL methanol for 2 h. The reaction resulted in a yellowish-brown precipitate that was filtered off and dried in vacuo (Scheme 1). The ligand was characterized using $^1\text{H-NMR}$ and ^{13}C nmR (See Figures S15 and S16). Anal. Calcd. For $\text{C}_9\text{H}_{11}\text{N}_3\text{O}_3$: C, 51.67; H, 5.30; N, 20.09. Found: C, 51.72; H, 5.58; N, 20.25.

3.3. Copper(II) Complex

The complex was formed from the reaction of ligands in DMF with a stirred solution of $\text{Cu}(\text{NO}_3)_2 \cdot 3\text{H}_2\text{O}$ (0.001 mol) in hot water. Then, sodium acetate (1 g) was incorporated into the mixture and refluxed for 1 h. A deep green color precipitate of the complex has resulted (Scheme 1). After filtering, the product was dried and used for testing.

Yield: 80%. Sum formula $\text{C}_{22}\text{H}_{26}\text{Cu}_2\text{N}_6\text{O}_{10}$; FTIR bands (KBr, cm^{-1} ; vs. = very strong, s = strong, br = broad, m = medium): 3250 (m), 2810 (m), 1656 (vs). UV-vis spectra [λ_{max} , nm (ϵ , $\text{L mol}^{-1}\text{cm}^{-1}$); MeOH (74 μM): 274 (7682) and 319 (4814). Anal. Calcd. For $\text{C}_{22}\text{H}_{24}\text{Cu}_2\text{N}_6\text{O}_{10}$: C, 40.06; H, 3.67; N, 12.74. Found: C, 40.19; H, 3.74; N, 12.67.

3.4. Physical Measurements

Physical measurements such as FTIR, UV, and mass of the complex were performed at Shimadzu IR Affinity (1S spectrometer) using a UV-vis spectrophotometer (Systronic, Gujarat, India), and mass spectrometer (Waters XEVO G2-XS QTOF, Waters, Milford, United States), respectively.

3.5. Theoretical Studies

The details of DFT and molecular docking have been shifted in supporting information (See the Supplementary Materials).

3.6. Stability Evaluation

For in vitro cytotoxic studies and DNA/BSA binding interaction studies, it is essential to check the complex stability in aqueous medium. Electronic absorption spectra of the complex in HEPES buffer for different times (day 1–5, and day 10) were performed to evaluate its stability in an aqueous solution. The experiments showed that there are almost no changes in the absorption maximum confirming its stability in the solution phase for a long period (Supplementary Figure S1).

3.7. Lipophilicity Check

The lipophilicity value for the molecules was determined in terms of $\log P_{\text{o/w}}$ (partition coefficient between n-octanol and water), involving the flask-shaking technique [36]. By taking 0.0023 g of the complex into 10 mL of octanol-water mixture (1:1 v/v) at room temperature. After allowing the solution to stand, the two phases (aqueous and octanol) became separated, and the complex concentration in both the phases was calculated through

Beer–Lambert law. With these concentrations, the lipophilicity value of the complex was achieved using the $\log P_{o/w} = \log ([\text{complex}]_{\text{octanol phase}} / [\text{complex}]_{\text{water phase}})$ equation.

3.8. DNA Binding

An absorption titration experiment was performed on a particular concentration of the complex (74 μM) upon the addition of CT-DNA (0–11.66 μM) in the HEPES buffer medium. For the intrinsic binding constant (K_{ib}), the following Wolfe–Shimmer Equation has been followed.

$$[\text{DNA}] \times (\varepsilon_a - \varepsilon_f)^{-1} = [\text{DNA}] \times (\varepsilon_b - \varepsilon_f)^{-1} + K_{ib}^{-1} \times (\varepsilon_b - \varepsilon_f)^{-1} \quad (8)$$

where ε_a , ε_f , and ε_b represent extinction coefficients of the complex, CT-DNA, and the bound complex, respectively. The ratio of the slope to intercept in the plot ($[\text{DNA}] / (\varepsilon_a - \varepsilon_f)$) vs. $[\text{DNA}]$ represents the K_{ib} value.

A Shimadzu RF-6000 Spectrofluorophotometer was used to record fluorometric titration at wavelengths of 200–700 nm, wherein the complex's emission intensity was seen as the CT-DNA concentration increased.

3.9. Interaction with BSA

This interaction study was performed using both absorption and emission spectroscopic techniques. The complex's absorbance at 319 nm changed, with increasing concentrations of BSA (0–0.34 μM) recorded.

For fluorescence emission, the changes were recorded at 334–336 nm, with a gradual increase in complex concentrations (0–12.3 μM).

3.10. Cytotoxicity

3.10.1. Culture and Maintenance of SiHa Cells

The cervical cancer cell lines (SiHa) were purchased from the National Centre for Cell Sciences (NCCS), Pune, India. Components of cell culture media viz. MTT (3-(4,5-Dimethylthiazol-2-yl)-2,5-diphenyltetrazolium bromide), Dulbecco's Modified Eagle Medium (DMEM), trypsin, Penicillin-Streptomycin-neomycin (PSN) antibiotic cocktail, and ethylenediaminetetraacetic acid (EDTA) were procured from HighMedia Biosciences, Bengaluru, India. Fetal bovine serum (FBS) was obtained from Thermo Fischer Scientific, India.

The cells were cultured in Dulbecco's Modified Eagle Medium (DMEM) supplemented with 10% heat-inactivated fetal bovine serum (FBS), 100 U/mL penicillin, and 100 $\mu\text{g}/\text{mL}$ streptomycin at 310 K. The temperature was preserved during the culture process in a humidified atmosphere (5% CO_2 supply).

3.10.2. Viability of the Cells

The MTT assay (3-(4,5-dimethylthiazol-2-yl)-2,5-diphenyltetrazolium bromide) was utilized to assess the viability of the cells. Approximately 70–80% of cells were seeded with 0.1 mL of DMEM comprising 10% fetal bovine serum, 50 U/mL penicillin, and 50 $\mu\text{g}/\text{mL}$ streptomycin. The wells were then incubated at 310 K in 5% CO_2 . All the treatments were performed in triplicate to obtain reproducible data. Thereafter, 100 μL of fresh medium was added to each well to remove the dead cells. To create water-insoluble formazan, 0.5 mg/mL of MTT solution in DMEM was placed in each well, and kept for incubation for 3 h at 310 K. To solubilize this formazan, each well was filled with DMSO, and the absorbance was measured at 570 nm using a microplate reader. The percentage of cell viability was evaluated by the formula.

$$\% \text{ Cell viability} = \frac{\text{OD of Test}}{\text{OD of Control}} \quad (9)$$

where OD stands for the specimen's optical density.

3.10.3. Fluorescence Imaging

A fluorescence microscopic examination was used to see how the specimen's cell efficiency proliferated. To eliminate floating or dead cells, test samples were twice rinsed with new phosphate buffer saline (PBS). After fixing adhered cells for 20 min with a 4% paraformaldehyde solution, they were again rinsed with PBS. Samples were stained for 10 min using the fluorescent dyes (AO and EB) (100 µg/mL). They were then twice washed with PBS and incubated for an additional 5 min in the dark. A Leica fluorescence microscope (Germany) was used to capture the images.

4. Conclusions

The current study highlights the significant cytotoxic potential of the newly synthesized binuclear copper (II) complex against SiHa cancer cells. The complex of (E)-2-(1-(2,4-dihydroxyphenyl)ethylidene)hydrazine-1-carboxamide has been validated through matching of DFT-simulated and experimental IR spectra. The complex is stable in a buffer solution and it is significantly lipophilic. Various spectroscopic techniques were employed to investigate the complex's binding to DNA and BSA. The experimental outcomes revealed that the complex binds to CT-DNA via partial intercalation and in a hydrophobic manner. However, the complex interacts with BSA predominantly by hydrogen bonding or van der Waals interactions rather than hydrophobic interactions. Furthermore, molecular docking investigations support the location of the complex inside the DNA and BSA protein. From the cell viability studies, it was observed that the complex demonstrates *in vitro* anti-proliferative activities against SiHa cancerous cells. The lipophilic character and the strong binding affinity with DNA and BSA may be accountable for the cytotoxicity of the complex against cancerous cells and demonstrate its scope in chemotherapeutics as an anti-proliferative candidate.

Supplementary Materials: The following supporting information can be downloaded at: <https://www.mdpi.com/article/10.3390/inorganics12010019/s1>. Figure S1 Electronic absorption spectra of the complex in HEPES buffer for different times (Day 1, Day 2, Day 5 and Day 10). Figure S2 Electronic absorption spectrum of the ligand. Figure S3 (a) FTIR spectrum of the complex (b) The experimental and DFT-simulated IR spectroscopy of the complex (c) FTIR spectrum of the ligand. Figure S4 ESI-MS spectrum of the complex. Figure S5 Fluorescence displacement assay of the complex by EB. Figure S6 Fluorescence displacement assay of the complex by Hoechst. Figure S7 Melting temperature of CT-DNA with and without the complex. Figure S8 Relative viscosities of the CT-DNA-EB, CT-DNA-Hoechst and CT-DNA-complex solutions with increasing amounts of EB or complex or Hoechst (0.01–0.05 µM). Figure S9 Plot of association constants (K_b) of complex and CT-DNA adduct against concentration of NaCl [25–100 µM]. Figure S10 Effect of the addition of complex on the emission intensity of BSA at 298, 303 and 308 K. Figure S11 Stern volmer plots for fluorescence quenching of BSA at 298, 303 and 308 K. Figure S12 Plot of $\log((F_0 - F)/F)$ versus $\log[\text{complex}]$ at 298, 303 and 308 K for binding interaction of BSA with the complex. Figure S13 Plot of $\ln K_b$ versus $1/T$ for BSA binding with the complex. Figure S14 Day wise percentage of cell viability. Figure S15 ^1H nmR of ligand. Figure S16 ^{13}C nmR of ligand. Table S1 Cu-O and Cu-N bond lengths in the complex. Table S2 Experimental and DFT-simulated IR spectroscopy data of the complex. Table S3 Enhancement constants of DNA and complex interaction. Table S4 Binding parameters of BSA and complex interaction.

Author Contributions: Conceptualization, B.C.S. and N.S.; methodology, R.M. and B.M.; validation, S.M. and N.S.; formal analysis, K.J.; investigation, N.S. and T.M.; data curation, R.M., K.J. and S.M.; writing—original draft preparation, B.C.S. and N.S.; writing—review and editing, M.A.; visualization, K.J., R.M. and N.S.; supervision, B.C.S.; funding acquisition, B.C.S. and M.A. All authors have read and agreed to the published version of the manuscript.

Funding: Dr. Bidhan Chandra Samanta sincerely acknowledges the financial assistance from DBT, Govt. of India (Order No HRD-11011/161/2020-HRD-DBT, Dated 24 August 2020). Dr. Mohd. Afzal received financial support from Researchers Supporting Project number (RSPD2024R979), King Saud University, Riyadh, Saudi Arabia.

Institutional Review Board Statement: Not applicable.

Informed Consent Statement: Not applicable.

Data Availability Statement: The original contributions presented in the study are included in the article/Supplementary Materials; further inquiries can be directed to the corresponding authors.

Acknowledgments: Bidhan Chandra Samanta sincerely acknowledges the financial assistance from DBT, Govt. of India to Mugberia Gangadhar Mahavidyalaya under Star College Strengthening Scheme (Order No HRD-11011/161/2020-HRD-DBT, Dated 24/08/2020). Kind assistance from Pralay Maiti, IIT, BHU is gratefully acknowledged. Nayim Sepay wishes to acknowledge Lady Brabourne College, Kolkata for laboratory facilities. Mohd. Afzal acknowledges Researchers Supporting Project number (RSPD2024R979), King Saud University, Riyadh, Saudi Arabia, for financial assistance.

Conflicts of Interest: The authors declare no conflict of interest.

References

1. Wang, D.; Lippard, S.J. Cellular processing of platinum anticancer drugs. *Nat. Rev. Drug Discov.* **2005**, *4*, 307–320. [[CrossRef](#)] [[PubMed](#)]
2. Marques, M.P.M. Platinum and Palladium Polyamine Complexes as Anticancer Agents: The Structural Factor. *ISRN Spectrosc.* **2013**, *2013*, 287353. [[CrossRef](#)]
3. Abu-Surrah, A.; Kettunen, M. Platinum Group Antitumor Chemistry: Design and development of New Anticancer Drugs Complementary to Cisplatin. *Curr. Med. Chem.* **2006**, *13*, 1337–1357. [[CrossRef](#)] [[PubMed](#)]
4. Karami, K.; Mehri Lighvan, Z.; Alizadeh, A.M.; Poshteh-Shirani, M.; Khayamian, T.; Lipkowski, J. Synthesis of a novel trinuclear palladium complex: The influence of an oxime chelate ligand on biological evaluation towards double-strand DNA, BSA protein and molecular modeling studies. *RSC Adv.* **2016**, *6*, 78424–78435. [[CrossRef](#)]
5. Raman, N.; Dhaveethu Raja, J.; Sakthivel, A. Synthesis, spectral characterization of Schiff base transition metal complexes: DNA cleavage and antimicrobial activity studies. *J. Chem. Sci.* **2007**, *119*, 303–310. [[CrossRef](#)]
6. Ott, I.; Gust, R. Non Platinum Metal Complexes as Anti-cancer Drugs. *Arch. Pharm.* **2007**, *340*, 117–126. [[CrossRef](#)]
7. Belicchi Ferrari, M.; Bisceglie, F.; Gasparri Fava, G.; Pelosi, G.; Tarasconi, P.; Albertini, R.; Pinelli, S. Synthesis, characterization and biological activity of two new polymeric copper(II) complexes with α -ketoglutaric acid thiosemicarbazone. *J. Inorg. Biochem.* **2002**, *89*, 36–44. [[CrossRef](#)]
8. Ranford, J.D.; Sadler, P.J.; Tocher, D.A. Cytotoxicity and antiviral activity of transition-metal salicylato complexes and crystal structure of Bis(diisopropylsalicylato)(1,10-phenanthroline)copper(II). *J. Chem. Soc. Dalt. Trans.* **1993**, *22*, 3393. [[CrossRef](#)]
9. Nonkuntod, P.; Boonmak, J.; Senawong, T.; Soikum, C.; Chaveerach, P.; Watwiangkham, A.; Suthirakun, S.; Chaveerach, U. The effect of gallic acid on the copper(ii) complex of *N*-(methylpyridin-2-yl)-amidino-*O*-methylurea: Crystal structure, DNA interactions, in vitro cytotoxicity and antibacterial activity. *New J. Chem.* **2023**, *47*, 12259–12273. [[CrossRef](#)]
10. Vilar, S.; Costanzi, S. Predicting the Biological Activities Through QSAR Analysis and Docking-Based Scoring. In *Membrane Protein Structure and Dynamics: Methods and Protocols*; Springer Nature: Berlin/Heidelberg, Germany, 2012; pp. 271–284.
11. Mir, I.A.; Ain, Q.U.; Qadir, T.; Malik, A.Q.; Jan, S.; Shahverdi, S.; Nabi, S.A. A review of semicarbazone-derived metal complexes for application in biomedicine and related fields. *J. Mol. Struct.* **2024**, *1295*, 136216. [[CrossRef](#)]
12. Liu, R.; Cui, J.; Ding, T.; Liu, Y.; Liang, H. Research Progress on the Biological Activities of Metal Complexes Bearing Polycyclic Aromatic Hydrazones. *Molecules* **2022**, *27*, 8393. [[CrossRef](#)] [[PubMed](#)]
13. Lee, P.F.; Yang, C.-T.; Fan, D.; Vittal, J.J.; Ranford, J.D. Synthesis, characterization and physicochemical properties of copper(II) complexes containing salicylaldehyde semicarbazone. *Polyhedron* **2003**, *22*, 2781–2786. [[CrossRef](#)]
14. Chen, R.; Liu, C.-S.; Zhang, H.; Guo, Y.; Bu, X.-H.; Yang, M. Three new Cu(II) and Cd(II) complexes with 3-(2-pyridyl)pyrazole-based ligand: Syntheses, crystal structures, and evaluations for bioactivities. *J. Inorg. Biochem.* **2007**, *101*, 412–421. [[CrossRef](#)] [[PubMed](#)]
15. Tabassum, S.; Al-Asbahy, W.M.; Afzal, M.; Arjmand, F.; Hasan Khan, R. Interaction and photo-induced cleavage studies of a copper based chemotherapeutic drug with human serum albumin: Spectroscopic and molecular docking study. *Mol. Biosyst.* **2012**, *8*, 2424. [[CrossRef](#)]
16. Maity, R.; Sepay, N.; Pramanik, U.; Jana, K.; Mukherjee, S.; Maity, S.; Mal, D.; Maity, T.; Samanta, B.C. Exploring the Noncovalent Interactions of the Dinuclear Cu(II) Schiff Base Complex with Bovine Serum Albumin and Cell Viability against the SiHa Cancer Cell Line. *J. Phys. Chem. B* **2021**, *125*, 11364–11373. [[CrossRef](#)]
17. Hansch, C.; Björkroth, J.P.; Leo, A. Hydrophobicity and Central Nervous System Agents: On the Principle of Minimal Hydrophobicity in Drug Design. *J. Pharm. Sci.* **1987**, *76*, 663–687. [[CrossRef](#)]
18. Ghose, A.K.; Viswanadhan, V.N.; Wendoloski, J.J. A Knowledge-Based Approach in Designing Combinatorial or Medicinal Chemistry Libraries for Drug Discovery. 1. A Qualitative and Quantitative Characterization of Known Drug Databases. *J. Comb. Chem.* **1999**, *1*, 55–68. [[CrossRef](#)]
19. Tian, N.; Zhou, Z.-Y.; Sun, S.-G.; Ding, Y.; Wang, Z.L. Synthesis of Tetrahedral Platinum Nanocrystals with High-Index Facets and High Electro-Oxidation Activity. *Science* **2007**, *316*, 732–735. [[CrossRef](#)]

20. Cox, P.J.; Psomas, G.; Bolos, C.A. Characterization and DNA-interaction studies of 1,1-dicyano-2,2-ethylene dithiolate Ni(II) mixed-ligand complexes with 2-amino-5-methyl thiazole, 2-amino-2-thiazoline and imidazole. Crystal structure of [Ni(i-MNT)(2a-5mt)₂]. *Bioorg. Med. Chem.* **2009**, *17*, 6054–6062. [[CrossRef](#)]
21. Jana, K.; Maity, R.; Puschmann, H.; Mitra, A.; Ghosh, R.; Debnath, S.C.; Shukla, A.; Mahanta, A.K.; Maity, T.; Samanta, B.C. A binuclear chloride bridged Cu(II) and a mononuclear Ni(II) complex: Synthesis, crystal structure, photo catalytic and biological studies. *Inorganica Chim. Acta* **2021**, *515*, 120067. [[CrossRef](#)]
22. Shahabadi, N.; Kashanian, S.; Darabi, F. In Vitro Study of DNA Interaction with a Water-Soluble Dinitrogen Schiff Base. *DNA Cell Biol.* **2009**, *28*, 589–596. [[CrossRef](#)] [[PubMed](#)]
23. Abdel-Rahman, L.H.; Abu-Dief, A.M.; El-Khatib, R.M.; Abdel-Fatah, S.M. Sonochemical synthesis, DNA binding, antimicrobial evaluation and in vitro anticancer activity of three new nano-sized Cu(II), Co(II) and Ni(II) chelates based on tri-dentate NOO imine ligands as precursors for metal oxides. *J. Photochem. Photobiol. B Biol.* **2016**, *162*, 298–308. [[CrossRef](#)] [[PubMed](#)]
24. Lakshmi-praba, J.; Arunachalam, S.; Riyasdeen, A.; Dhivya, R.; Akbarsha, M.A. Polyethyleneimine anchored copper(II) complexes: Synthesis, characterization, in vitro DNA binding studies and cytotoxicity studies. *J. Photochem. Photobiol. B Biol.* **2015**, *142*, 59–67. [[CrossRef](#)] [[PubMed](#)]
25. Ünver, H.; Boyacıoğlu, B.; Zeyrek, C.T.; Yıldız, M.; Demir, N.; Yıldırım, N.; Karaosmanoğlu, O.; Sivas, H.; Elmali, A. Synthesis, spectral and quantum chemical studies and use of (E)-3-[(3,5-bis(trifluoromethyl)phenylimino)methyl]benzene-1,2-diol and its Ni(II) and Cu(II) complexes as an anion sensor, DNA binding, DNA cleavage, anti-microbial, anti-mutagenic and anti-ca. *J. Mol. Struct.* **2016**, *1125*, 162–176. [[CrossRef](#)]
26. Rajendiran, V.; Karthik, R.; Palaniandavar, M.; Stoeckli-Evans, H.; Periasamy, V.S.; Akbarsha, M.A.; Srinag, B.S.; Krishnamurthy, H. Mixed-Ligand Copper(II)-phenolate Complexes: Effect of Coligand on Enhanced DNA and Protein Binding, DNA Cleavage, and Anticancer Activity. *Inorg. Chem.* **2007**, *46*, 8208–8221. [[CrossRef](#)] [[PubMed](#)]
27. Ross, P.D.; Subramanian, S. Thermodynamics of protein association reactions: Forces contributing to stability. *Biochemistry* **1981**, *20*, 3096–3102. [[CrossRef](#)]
28. Das, S.; Kumar, G.S. Molecular aspects on the interaction of phenosafranine to deoxyribonucleic acid: Model for intercalative drug–DNA binding. *J. Mol. Struct.* **2008**, *872*, 56–63. [[CrossRef](#)]
29. Kumar, C.V.; Turner, R.S.; Asuncion, E.H. Groove binding of a styrylcyanine dye to the DNA double helix: The salt effect. *J. Photochem. Photobiol. A Chem.* **1993**, *74*, 231–238. [[CrossRef](#)]
30. García-Giménez, J.L.; Alzuet, G.; González-Álvarez, M.; Liu-González, M.; Castiñeiras, A.; Borrás, J. Oxidative nuclease activity of ferromagnetically coupled μ -hydroxo- μ -propionato copper(II) complexes [Cu₃(L)₂(μ -OH)₂(μ -propionato)₂] (L=N-(pyrid-2-ylmethyl)R-sulfonamidato, R=benzene, toluene, naphthalene). *J. Inorg. Biochem.* **2009**, *103*, 243–255. [[CrossRef](#)]
31. Sirajuddin, M.; Ali, S.; Badshah, A. Drug–DNA interactions and their study by UV–Visible, fluorescence spectroscopies and cyclic voltametry. *J. Photochem. Photobiol. B Biol.* **2013**, *124*, 1–19. [[CrossRef](#)]
32. Record, M.T.; Anderson, C.F.; Lohman, T.M. Thermodynamic analysis of ion effects on the binding and conformational equilibria of proteins and nucleic acids: The roles of ion association or release, screening, and ion effects on water activity. *Q. Rev. Biophys.* **1978**, *11*, 103–178. [[CrossRef](#)] [[PubMed](#)]
33. Lian, W.-J.; Wang, X.-T.; Xie, C.-Z.; Tian, H.; Song, X.-Q.; Pan, H.-T.; Qiao, X.; Xu, J.-Y. Mixed-ligand copper(II) Schiff base complexes: The role of the co-ligand in DNA binding, DNA cleavage, protein binding and cytotoxicity. *Dalt. Trans.* **2016**, *45*, 9073–9087. [[CrossRef](#)] [[PubMed](#)]
34. Sepay, N.; Banerjee, M.; Islam, R.; Dey, S.P.; Halder, U.C. Crystallography based exploration of non-covalent interactions to design, synthesis of coumarin for stronger protein binding. *Phys. Chem. Chem. Phys.* **2022**, *11*, 6605–6615. [[CrossRef](#)] [[PubMed](#)]
35. Margiotta, N.; Natile, G.; Capitelli, F.; Fanizzi, F.P.; Boccarelli, A.; De Rinaldis, P.; Giordano, D.; Coluccia, M. Sterically hindered complexes of platinum(II) with planar heterocyclic nitrogen donors. A novel complex with 1-methyl-cytosine has a spectrum of activity different from cisplatin and is able of overcoming acquired cisplatin resistance. *J. Inorg. Biochem.* **2006**, *100*, 1849–1857. [[CrossRef](#)]
36. Jagadeesan, S.; Balasubramanian, V.; Baumann, P.; Neuburger, M.; Häussinger, D.; Palivan, C.G. Water-Soluble Co(III) Complexes of Substituted Phenanthrolines with Cell Selective Anticancer Activity. *Inorg. Chem.* **2013**, *52*, 12535–12544. [[CrossRef](#)]

Disclaimer/Publisher’s Note: The statements, opinions and data contained in all publications are solely those of the individual author(s) and contributor(s) and not of MDPI and/or the editor(s). MDPI and/or the editor(s) disclaim responsibility for any injury to people or property resulting from any ideas, methods, instructions or products referred to in the content.